SUMMARY REPORT OF:

REAL-TIME CONTROL OF LEAN BLOWOUT AND NOX EMISSIONS IN A TURBINE ENGINE

NASA Grant NAG 2-1615

SUBMITTED BY: GEORGIA INSTITUTE OF TECHNOLOGY
SCHOOL OF AEROSPACE ENGINEERING

POINT OF CONTACT: PROFESSOR BEN ZINN
SCHOOL OF AEROSPACE ENGINEERING
ATLANTA, GA. 30332 – 0150
(404) 894-3033
(404) 894 – 2760, FAX
ben.zinn@aerospace.gatech.edu

I. EXECUTIVE SUMMARY

This report describes research on the development and demonstration of a *controlled combustor* operates with *minimal NO_x emissions*, thus meeting one of NASA's UEET program goals. In a previous NASA-supported program, NO_x emissions were successfully minimized by operating a premixed, lean burning combustor (modeling a lean prevaporized, premixed LPP combustor) *safely* near its lean blowout (LBO) limit over a range of operating conditions. This was accomplished by integrating the combustor with an LBO precursor sensor and closed-loop, rule-based control system that allowed the combustor to operate far closer to the point of LBO than an uncontrolled combustor would be allowed to in a current engine. Since leaner operation generally leads to lower NO_x emissions, engine NO_x could be reduced. That work was extended here to a more conventional (nonpremixed), liquid fueled combustor configuration. The active control system prevents LBO from leading to flame loss, and utilizes actuators to reduce NO_x emissions at various power levels. In the long term, this will allow engine designers to improve the passive design of the combustor, by removing constraints associated with infrequent but important operating conditions. Specifically, the following were achieved.

First, we demonstrated acoustic and optic based sensing for LBO and NOx control in liquid-fueled, nonpremixed, aeroengine model combustor. To accomplish this we developed a single-cup, annular combustor utilizing a commercial CFM56 swirl cup inlet. The cooperated on standard (commercial) Jet-A fuel and the inlet air was electrically preheated (~300 °F) to simulate the aircraft compressor exhaust. The optical precursor sensing (based on detection of ultraviolet chemiluminescence from OH and extinction event identification from robust thresholding techniques) was successfully demonstrated in this liquid-fueled aeroengine model combustor using fiber-optics and remotely located, rugged sensors. In addition, we demonstrated robust LBO precursor sensing using wavelet and bandpass filtering of acoustic (pressure) signals combined with the threshold event identification technique. Finally, we examined sensor fusion methodologies for jointly analyzing these acoustic and optic data in order to determine more accurate, robust, and noise-insensitive LBO precursor detection methods.

Next, we examined fuel-based control for preventing LBO and decreasing overall NOx emissions in the liquid-fueled combustor. The system included: 1) optical and/or acoustic sensing and identification of LBO precursors based on short-duration extinction events that occur before the blowout condition is reached; and 2) pilot and main fuel control to allow for stabilizing the flame without altering the power setting.

Finally, this research led to two invention disclosures for the control system and the developed advanced filtering schemes.

II. MOTIVATION AND OBJECTIVES

This aim of this research program was to develop and demonstrate a ***control system for aeroengine combustors*** that will operate with ***minimal NO_x emissions*** by operating a "lean" burning combustor ***without risk of blowout*** over a range of operating conditions, e.g., altitude and power setting. The closed-loop control system should allow operation far closer to the point of lean blowout (LBO) than would be possible in an uncontrolled combustor. Since leaner operation leads to lower NO_x emissions, the NO_x levels would be significantly reduced. In addition, the control system would allow the engine designer to improve the overall engine design by removing the constraint of completely avoiding (infrequent) operating conditions that would lead to blowout without the control system present.

II.A Low Emissions Combustors

A number of approaches have been investigated for lowering NO_x emissions. For example, lean burning combustors offer great promise for reducing NO_x emissions. In so-called LPP combustors (*L*ean *P*revaporized *P*remixed), the fuel is quickly atomized, mixed with heated air and vaporized before entering the combustion zone in order to achieve lean premixed combustion. This mode of burning has significant advantages over its nonpremixed counterpart in achieving low pollutant emissions, particularly in regards to NO_x and soot.[1]

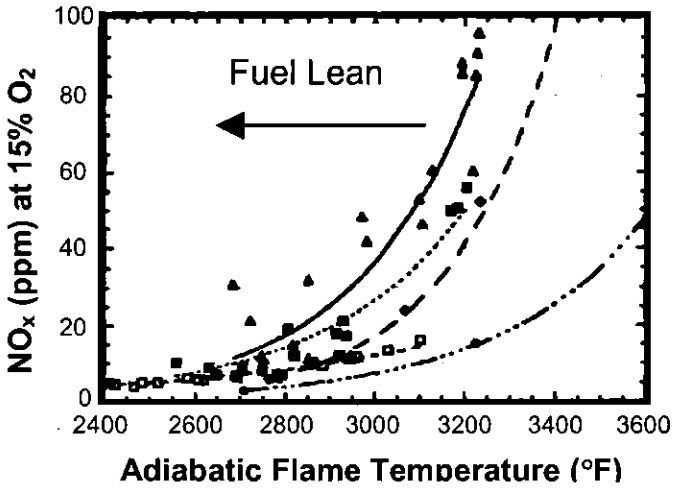

Figure 1. NO_x emission results for various aero-engine, lean-burning (prevaporized fuel) combustors.[2] Generally, lower adiabatic flame temperatures are achieved by using a more fuel lean mixture.

For example, Fig. 1 shows NO_x emissions from premixed combustors operating with various fuel-air ratios. As the equivalence ratio is lowered (leaner operation), the adiabatic flame temperature drops and the NO_x emissions are reduced. For partially premixed combustors, which have at least some regions of the combustor that achieve peak temperatures close to the stoichiometric/maximum value, NO_x emission levels are typically controlled by the thermal (Zeldovich) mechanism.[3] On the other hand, a well-designed LPP combustor can produce ultralow NO_x levels, with the lower limit dependent on the prompt (Fenimore) or N_2O mechanisms, rather than the higher temperature Zeldovich mechanism.[3] However, lean burning

combustors are also prone to transient flame holding issues, such as inability to stabilize the flame in the combustor[4] and flashback into the prevaporizer section.

II.B Lean Blowout

A significant issue for both LPP and conventional (partially premixed) combustors is flame stability during lean operation, i.e., lean blowout, which can result in a severe operability loss. Flame stabilization involves competition between the rates of the chemical reactions and the rates of turbulent advection and diffusion of species and energy to and from the flame, and includes local ignition and extinction behavior. As the equivalence (or fuel-air) ratio of a reaction zone is reduced, extinction events become more likely, and the lean limit for stable operation may be reached. For example, Fig. 2 shows a nominal stability curve for a premixed combustor. The combustor loading parameter is a function of the reactant flow rate and combustor size. In a conventional combustor, LBO can typically occur when the fuel flowrate is reduced too rapidly compared to the compressor response time. If the compressor spools down too slowly, the air flow remains high while the fuel is reduced, leading to lean operation. Thus LBO in a conventional combustor can also limit engine deceleration rate.

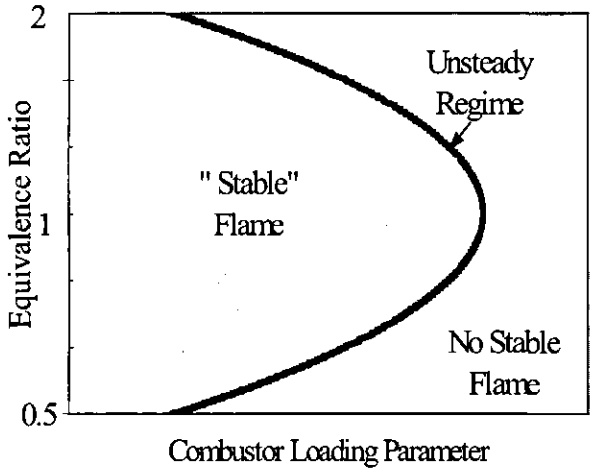

Figure 2. Characteristic stability map for a premixed combustor showing regions where sustainable combustion is possible, i.e., to the left of the stability limit curve.

For an engine designer, the challenge is to develop a combustor that achieves stable operation and low NO_x emissions over the full range of engine conditions. Thus, the combustor designer must build enough margin into the design to prevent LBO at the worst case operating condition. Consequently, there can be an increase in NO_x production compared to what could be optimally achieved at other operating conditions. Furthermore, when coupled with overall engine system dynamics, flame blowout can result in the inability of an engine to recover from a compressor stall event.[5]

III. RESEARCH RESULTS AND ACCOMPLISHMENTS

III.A Liquid-Fueled Aeroengine Combustor

The combustor used in this study is a single-cup, annular geometry system based on a commercial aeroengine device (CFM-56). The burner head contains coannular (cylindrical), counter-rotating swirlers. The production model fuel injector, which is located at the center of the swirlers and upstream of the point where the two swirling flows meet, is replaced with a pressure-swirl atomizer for main fuel injection (see Figure 3). The fuel used for these experiments was Jet-A aviation grade petroleum. Air is supplied to the combustor from storage tanks (~1MPa storage pressure) and electrically preheated to approximately 380 K before entering the swirlers. The test-section (~81 cm^2) is optically accessible through quartz side walls. The inner sides of the top and bottom walls, as well as the burner head, are thermal barrier coated. The combustion gases exit through a small converging nozzle to provide a more realistic exit boundary condition.

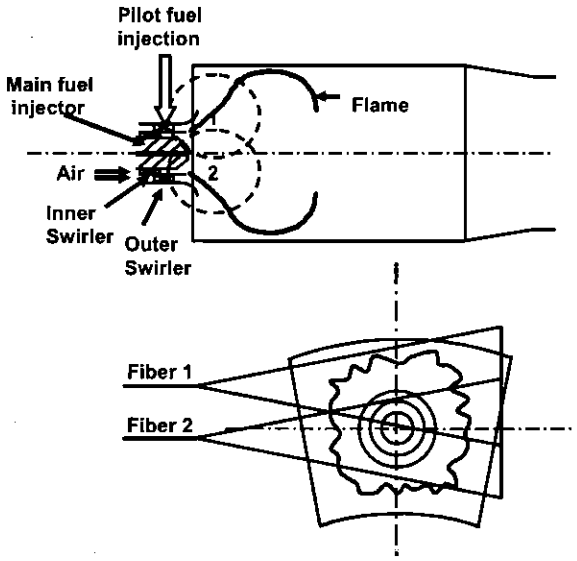

Figure 3. Combustor schematic, including the viewing areas for the optical fibers used.

For the current studies, the combustor was operated at atmospheric pressure with an air flowrate near 40 g/s and fuel rates of on the order of 1 g/s. This leads to an average axial velocity in the test section of ~20 m/s for the burned gases. When operated with an overall equivalence ratio of 0.4 under these flowrates, the chemical heat release rate is ~45 kW.

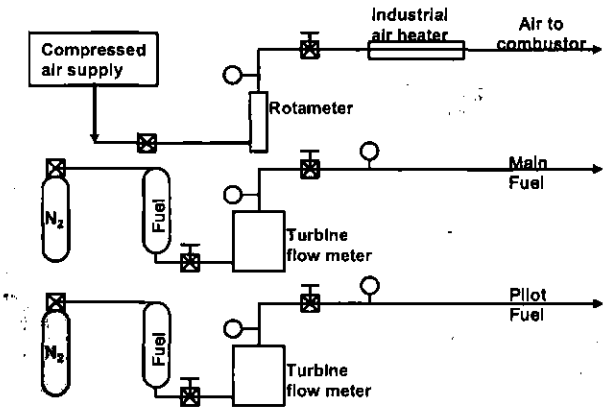

Figure 4. A schematic of the fuel and air flow control and monitoring system.

A schematic of the basic flow control system is shown in Figure 4. Variations in overall equivalence ratio were generally obtained by varying the fuel flow rate into the combustor. For operation without active-control there were separate, manually controlled, flow systems for the main and pilot fuel lines. The resolution of the turbine flow meters used to monitor the fuel flowrates corresponds to a change in equivalence ratio of 0.002.

III.B LBO Sensing

The sensing strategy for LBO precursors is based on the notion that flame blowout is preceded by a transient period. This period is marked by localized extinction and reignition events, and therefore irregular rates of fuel consuming reactions and the associated heat release. In addition, this leads to large-scale flame unsteadiness. These events can be detected either by: 1) **acoustic sensors**, which respond to the acoustic waves produced by the unsteady heat release, via **unsteady volumetric expansion**; or 2) **optical sensors** that respond to the unsteady reaction rate of elementary steps in the oxidation of the fuel that produce electronically excited molecules that can then fluoresce, i.e., produce **chemiluminescence**.

III.B.1 Optical Sensing

With respect to optical sensing, the primary chemiluminescent species of interest in a hydrocarbon flame are electronically excited OH, CH and C_2 radicals and the CO_2 molecule. In lean hydrocarbon flames, OH tends to be the strong emitter, followed by CH with little C_2 emission. As the equivalence ratio increases (more fuel rich), the CH and C_2 emission bands are relatively stronger. The present work uses chemiluminescence from OH (308nm) for detecting LBO precursor events, since the OH is strong, and because the UV spectrum has very little interference from blackbody radiation (from walls or particles). Together, these qualities (high signal-to-noise ratio and high signal-to-background ratio) make the OH signal the best choice in terms of observability. Also, optical methods inherently have a fast time response providing fast detection of flame instability events. Finally, optical sensing in general is applicable to a combustor, for example, using fiber optic ports on the combustor walls.

Experiments were conducted at various equivalence ratios near the LBO limit. Chemiluminescence signals from the jet-A fueled liquid combustor showed intermittent events occurring very close to LBO in a similar fashion as observed in the premixed combustor work. Figure 5 shows a comparison of the optical signals over a 0.6 second time frame from the

current, liquid-fueled combustor (from fiber 1 viewing the top portion of the combustor) and the previous (premixed) results. The signals have been normalized to facilitate the comparison.

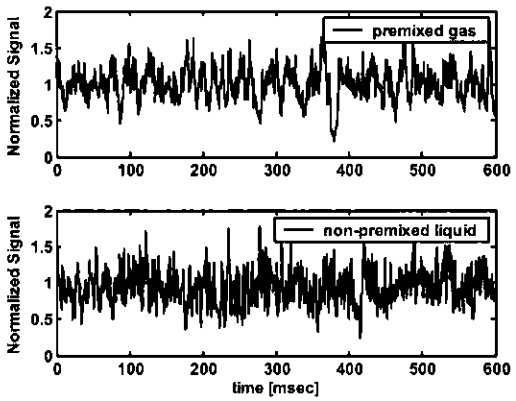

Figure 5. Time series normalized OH chemiluminescence signals showing LBO precursor events from a premixed gaseous fuel combustor and the nonpremixed aeroengine combustor.

Both signals exhibit a few, well-defined, partial extinction events. For example, the premixed data shows a significant drop in emission at ~380 msec, while the liquid data does something similar at ~410 msec. The most significant difference between the two combustors is the appearance of many short duration spikes in the liquid-fueled, aeroengine combustor. While there are some similar spikes in the premixed combustor data, there are significantly more of these in the aeroengine combustor. In addition, the amplitude of these high frequency spikes is greater in the aeroengine combustor. One might assume that these spikes are simply an indication of increased noise in the detection system. Though the mean signal from the liquid combustor was smaller than the mean of the premixed system, the increase in the amplitude of the short duration spikes is much larger than the change in the mean signals. Also, these fluctuations are much greater than the electronic noise of the detector. Therefore, it is unlikely the spikes (in either combustor) are due to shot-noise (which scales as the square-root of the mean signal) or detector noise.

Figure 6 shows two sequences of inverted grayscale images from a high speed visualization of the combustor. The conditions were nominally the same for the two cases. The gating time was 100 μsec. The images were rotated such that the top of the combustor appears on the right side of each image. Case (a) shows images that are from a stable combustion period. Case (b) shows a longer sequence which is during a partial flame loss event. In case (a), the sudden change in the intensity (third frame) happens within a 2-4 msec time scale. This sudden change in the intensity is the cause of the spikes noted before. These rapid fluctuations may be due to more intermittent combustion in the non-premixed combustor (compared to the premixed combustor), probably due to atomization non-uniformities or droplets burning individually in a diffusion mode. Thus the optical emission from the liquid-fueled aeroengine combustors has a higher natural intermittency and poses a greater challenge in terms of event identification (as described in the next section).

Case (b) shows a longer sequence showing a partial extinction event. The images are 15 msec apart. This sequence shows that temporarily there is an overall decrease in the intensity of the flame, but the top of the combustor exhibits greater flame loss than the bottom of the combustor. Thus the resultant flame appears to be present only in the bottom half of the combustor (left side

of the images). This behavior suggests that the combustor has a weaker stabilization near the top of the inlet section.

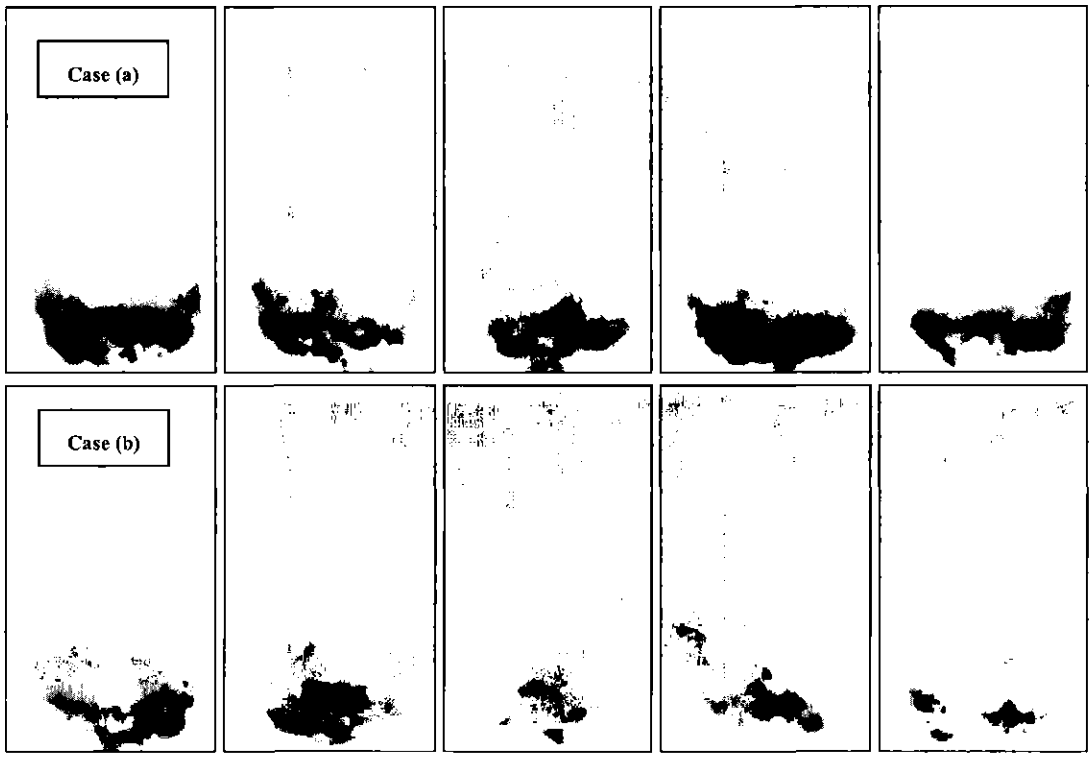

Figure 6. High speed visualization images (inverted grayscale) of a nominal flow condition: case (a) is sequence of images showing intermittency of combustion; time between images 2msec; case (b) shows a precursor event; time between images 15 msec. The images have been rotated such that the flow is upward, and the top of the combustor corresponds to the right side of the images.

The double threshold based method for identifying precursors, used in the previous (gaseous fuel) effort was adopted here. This method defines a start of a precursor event when the signal level drops below the lower threshold, and defines the end of the event when the signal level goes back above the upper threshold. The difference between lower and upper threshold is used to decrease the noise in the signal which can cause false/extra events. As the number of precursor events is expected to increase near blowout, it would be undesirable for the identification method to give extra events, as it might lead to erroneous conclusions about proximity to blowout. In the earlier work, the threshold values were defined to be a preset fraction of the local mean. For example, the signal dropping below 50% of the recent mean could start an event, which then ended when the signal went above 70% of the same mean. With the signal normalized by the recent mean, the event identification is robust with regard to long term variations in power setting, transmission efficiency of the optics and detector response.

The challenge in the liquid combustor is to find a method for setting the thresholds that takes into account the much larger degree of natural combustor intermittency. The approach chosen here is based on the recent statistics of the signal, in parallel to the mean normalization. Specifically, the threshold spacing is based on the recent standard deviation (σ) of the signal, which is primarily determined by the natural intermittency. So, the lower threshold, which begins

an event, was again defined to be 50% of the local mean, but the upper threshold was defined to be 2σ above the lower threshold (see Figure 7).

The choice of two standard deviations provides significant suppression of the intermittent spikes. For example, if the threshold difference was chosen to be one standard deviation, then there is a 30% chance the spikes would prematurely end the event (if the amplitude of the spikes is normally distributed). With a 2σ difference, there is only a 5% probability that any spike would prematurely end an event. This is illustrated in Figure 7, which shows a precursor event with a spike that crosses the 1σ line. Since the signal than falls below the 50% lower threshold almost immediately, the event identification scheme would find two events instead of one. The 2σ upper threshold does not have this problem. However, it should be noted that in this case, the 2σ threshold requires the signal to *rise above the mean.* While not a problem in the case shown in Figure 7, this could result in an artificially long duration event. Thus the optimum threshold separation may lie between 1σ and 2σ if σ is significant compared to the mean value (for example, more than one-fourth of the mean).

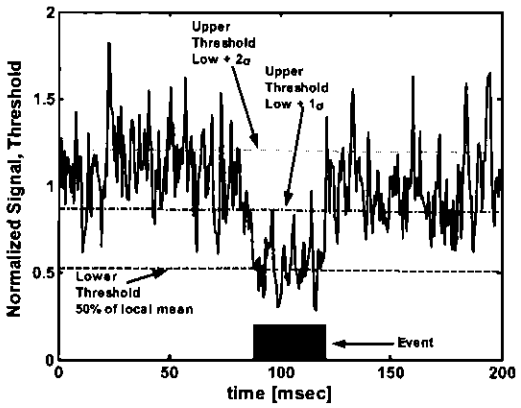

Figure 7. Illustration of the double threshold scheme showing the lower and upper thresholds with the signal, and the identified event.

Figure 8 shows how the events change with overall equivalence ratio as LBO is approached ($\phi_{LBO} \approx 0.385$ for the current conditions). Results are shown for both sensor locations. The average number of events per second (based on a 16 second data trace) tends to increase as the LBO limit is approached. Similarly, the average duration of an event also increases as the combustor becomes less stable. These trends are similar to that observed in the premixed combustor. This indicates that in both the premixed and non-premixed combustors, the proximity to LBO can be characterized by increased occurrence of temporary, local extinction events associated with fluctuations in combustor conditions. The increased duration of the events as one approaches LBO suggests that the extinguished fuel-air pockets may either become larger or harder to reignite or the rest of the combusting region is weaker and less able to reignite the gases.

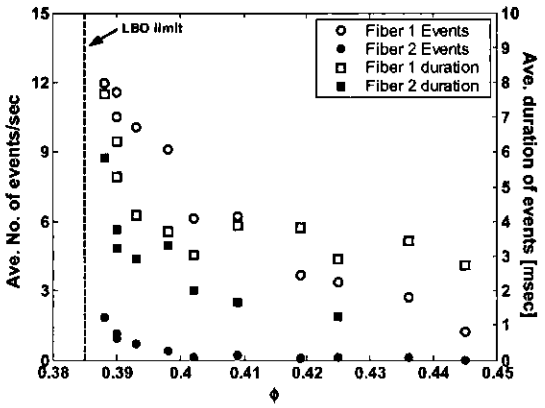

Figure 8. Variation of average number of events per second and the average duration of each event as a function of equivalence ratio. The dotted line indicates the LBO limit for the combustor.

One significant difference between the current results and the earlier (gaseous fuel) premixed data is the duration of the events, which are typically 2-5 times longer in the premixed combustor. There is also a large difference between the data from the two sensor locations in the liquid combustor. Fiber 1, which views the upper portion of the combustor, captures significantly more and longer events than the centerline sensor (see Figure 8). This indicates the flame is less stable (or "weaker") in upper location. This is also supported by the partial extinction of the flame on the top half of the images during the precursor event (see Figure 6).

The first point where the loss of stability occurs will most likely be the point where the stability is weakest, viz., the top of the combustor. It was observed that when the signal from fiber 2 indicates an extinction/precursor event, fiber 1 also detects the event most of the time. This suggests that events seen by fiber 2 may be more global compared to those seen by fiber 1. However, data from fiber 1 will likely be more sensitive to the approach of blowout compared to fiber 2 data in this combustor. Since partial flame loss events usually precede global flame loss precursors, it may be better to use data from fiber 1 for the purposes of early detection of proximity to blowout.

Thus, it is shown that the likelihood or duration of events increase with proximity to LBO. These parameters can therefore be useful in a control system to raise an alarm on the approach of blowout. For example, Figure 9 shows the time trace of number of events detected in a one second moving window for several equivalence ratios. This demonstrates the random occurrences of these events with the average number of events increasing as LBO limit is approached. A control system could programmed to respond when the number of events becomes significant. For example, if the event count from fiber 1 exceeds ten (or equivalently one count from fiber 2), the control system could engage an actuator to enhance the stabilization of the combustion process. This is the topic of the next section of the paper.

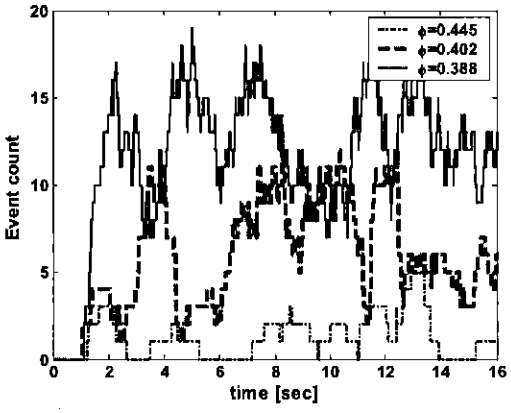

(a)

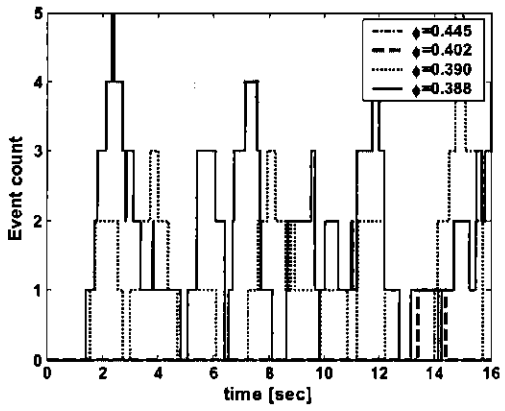

(b)

Figure 9. Event count in the previous 1 second, as a function of time for a few equivalence ratios (a) for the fiber 1 (b) for the bottom fiber 2.

III.B.2 Acoustic Sensing

Techniques for acoustic sensing were also improved under this effort, with part of the development utilizing the gas fueled combustor developed in the previous effort. Figure 10 plots typical measured time dependencies of the acoustic pressure at several normalized equivalence ratios, ϕ/ϕ_{LBO}=1.095, 1.014 and 1.001. Note the reduction in RMS pressure levels with equivalence ratio, due to the reduced heat release rates at the lower fuel flow rates. Near blowout, short time duration, high amplitude bursts are observed. These bursts coincide with the occurrence of the flame loss and re-ignition events described above.

CO emission measurements were also taken at the combustor exhaust to determine the dependence of combustion efficiency upon ϕ/ϕ_{LBO}. Although not shown, CO levels increased from ~75 to 350 ppm under stable and near blowout conditions, respectively. This large increase is partially due to the lengthening of the combustion zone to the point where it extends past the probe location point.

The combustion noise spectra of the swirl burner at three different normalized equivalence ratios, ϕ/ϕ_{LBO} = 1.095 and 1.001 are plotted in Figure 11. Each curve has been normalized to have the same total acoustic power in order to correct for the different fuel flow rates in each

case. Note that in the piloted burner case, the equivalence ratio and the total fuel flow rates changed minimally (<3%). As indicated in the figure, there is a marked increase in power in the 10-100 Hz spectral regime under these near flameout conditions. The low frequency increase is likely related to two time scales associated with the precursor events. The first time scale, 10-15 msec (hundreds of Hz), corresponds to the 'no flame' duration. The second time scale is the time between such events, which is around 1 sec or less (above a few Hz). Figure 12 plots the dependence of the acoustic power in the 10-100 Hz and 10-30 Hz frequency ranges normalized by the total power in the acoustic signal against normalized equivalence ratios. The power in these spectral bands increases by a factor of nearly 60 near blowout. Referring to Figure 11, it can be seen that the relative sensitivity of this ratio is comparatively constant below about 100 Hz, but rapidly diminishes at higher frequencies. Recall that the CO emissions increased by a factor of 5.

The acoustic data from the gas swirl burner were also examined using wavelet analysis. In order to increase sensitivity, "customized" wavelets were chosen which resembled the actual acoustic events close to blowout. The temporal characteristics of these events were determined from simultaneous analysis of OH chemiluminescence and the acoustic signal. Figure 13 shows a plot of acoustic (and optical data for comparison) at an equivalence ratio close to blowout. A detail of these data is also shown in the right half of Figure 13. The large dips in the optical signal suggest local temporary flame loss. A coincident feature is also evident in the acoustic signal, which resembles the derivative of the OH^* signal, as expected.

The following customized wavelet was generated, whose waveform is similar to the acoustic signature during these events:

$$W_3(t) = -\frac{d}{dt}(e^{-t^2/2}) \quad (5)$$

Figure 14 plots the computed $W_3(t)$ wavelet coefficients at a scale, ψ = 64, roughly corresponding to a frequency of 10 Hz. In contrast to the signal R.M.S., see Figure 10, the wavelet filtered R.M.S actually increases as the combustor approaches blowout. In addition, large amplitude bursts in the signal ("events") are increasingly obvious. Figure 15 plots the variance of the calculated W_3 (t) wavelet coefficients at scales, ψ = 64 and 4 that roughly corresponds to frequencies of 10 Hz and 125 Hz respectively. The figure shows that the power in the scale or "frequency" band increases by a factor of 60 and 40 respectively near blowout conditions. An important point to note is that other wavelet basis functions give very comparable results; i.e., the sensitivity of the change in variance upon basis function is minimal. This can be understood by noting that the wavelet filtering operation is equivalent to streaming the data through a pass-band filter. A straightforward application of Parseval's theorem shows that the variance of the filtered data will be quite similar for a variety of different wavelets whose Fourier transforms have similar center frequencies and bandwidths. What then is the advantage of identifying a "customized" wavelet? As we will show in the next section, the key advantage lies in the ability of the customized wavelet to accentuate the amplitude of time-localized events whose shape resembles that of the wavelet. As such, the choice of wavelet exerts a large impact upon the statistics of the filtered signal outliers (time-localized events) whose presence we are interested in detecting. As such, the key advantage in customized wavelets lie in using them in conjunction with a discrete event detection algorithm, such as level crossing approaches

(discussed in the next section), as opposed to a time-integrated detection algorithm, such as a variance calculation.

Thresholding the data provides a convenient way of converting data stream into a quantitative blowout indicator; e.g. a blowout avoidance logic can be invoked when the data exceed a threshold level a certain number of times. This is particularly useful for combustors that exhibit the presence of increasing number of time-localized "events" as blowout is approached.

The effect of threshold upon level crossing frequency can be understood from Figure 16, which plots the PDF of the $W_3(t)$ wavelet coefficients for ϕ/ϕ_{LBO} = 1.095, 1.014 and 1.001. The increased presence of high amplitude outliers close to blowout results in the long tail in the PDF. The figure indicates that the signal from the stable flames rarely exceeds ~30σ (i.e., 30 times the variance of the $W_3(t)$ coefficients for the stable combustion case). Figure 17 plots the dependence of 60σ level crossing frequency (number of crossings/second) and duration (time the signal exceeds the threshold/total time) upon ϕ/ϕ_{LBO}. The threshold level is also shown by the dashed lines in Figure 14. The number and duration of events rises from identically zero to about 5 events/sec and 150 msec/sec respectively just before blowout, as seen in Figure 17.

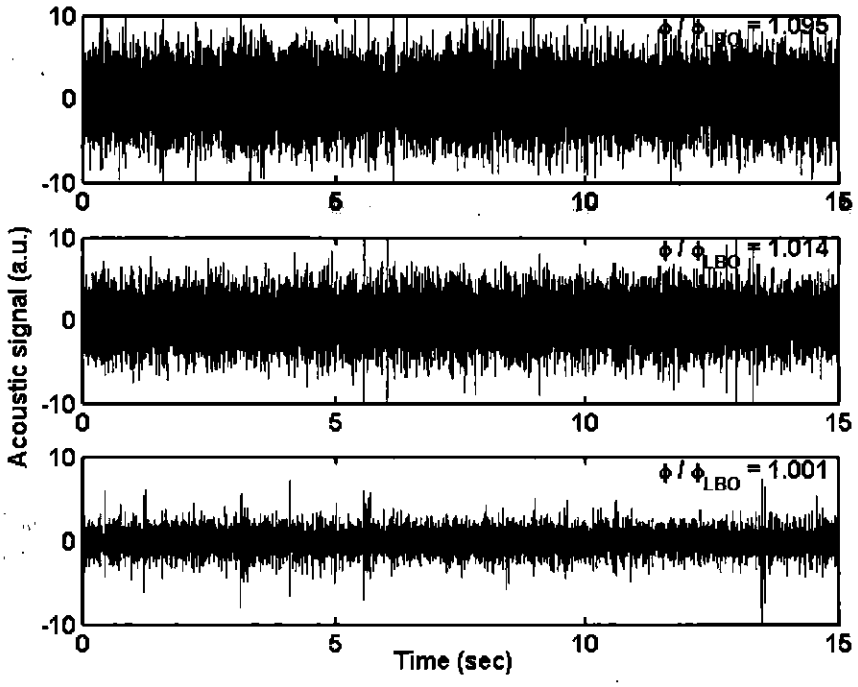

Figure 10. Acoustic signal from a swirl burner for ϕ/ϕ_{LBO} = 1.095, 1.014 and 1.001.

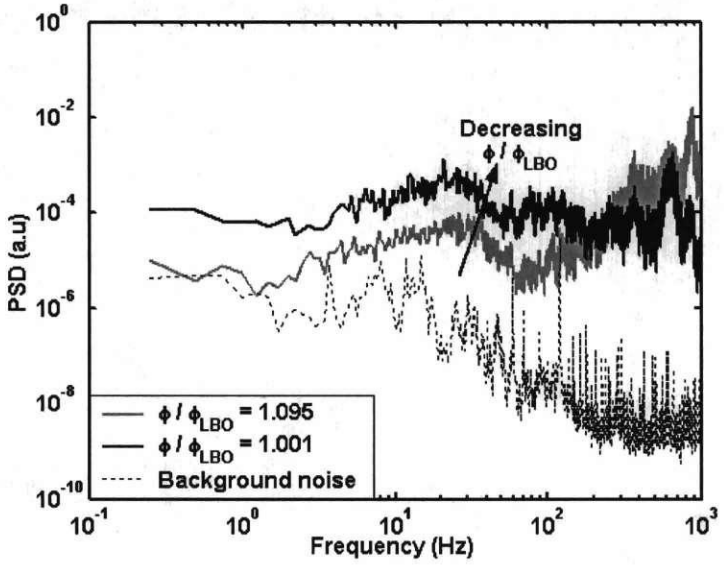

Figure 11. Normalized acoustic spectra of the background and reacting case (ϕ/ϕ_{LBO}= 1.095 and 1.001) for the swirl burner.

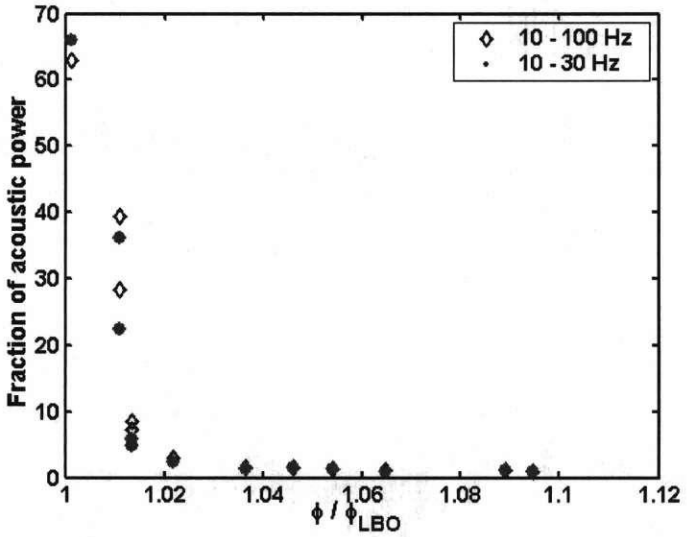

Figure 12. Dependence of the normalized acoustic power (scaled by the minima) in the swirl burner in the 10-100 Hz and 10-30 Hz frequency bands upon ϕ/ϕ_{LBO}.

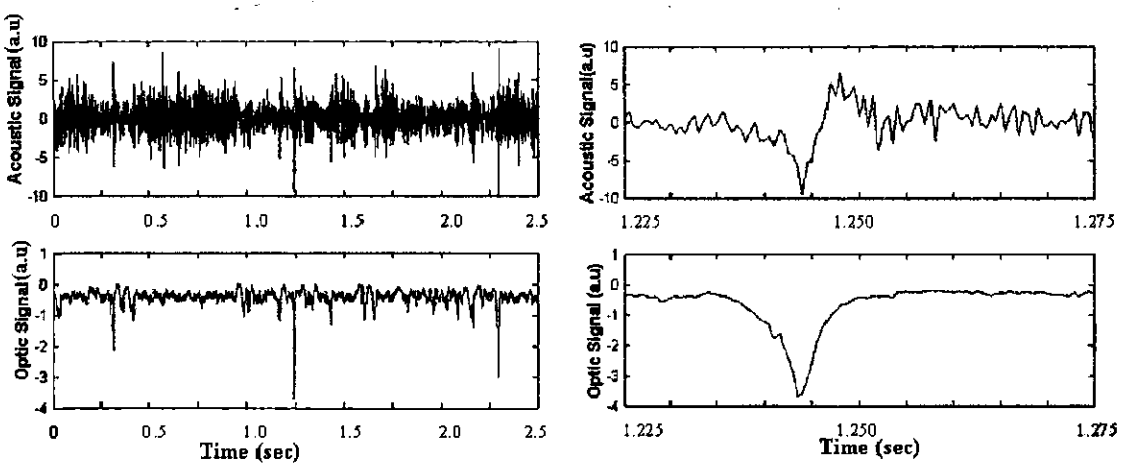

Figure 13. Acoustic and chemiluminescence time series data from the swirl burner for $\phi/\phi_{LBO} = 1.014$, close to blowout (left); and blown-up version of the blowout precursor in the acoustic and optic signal (right).

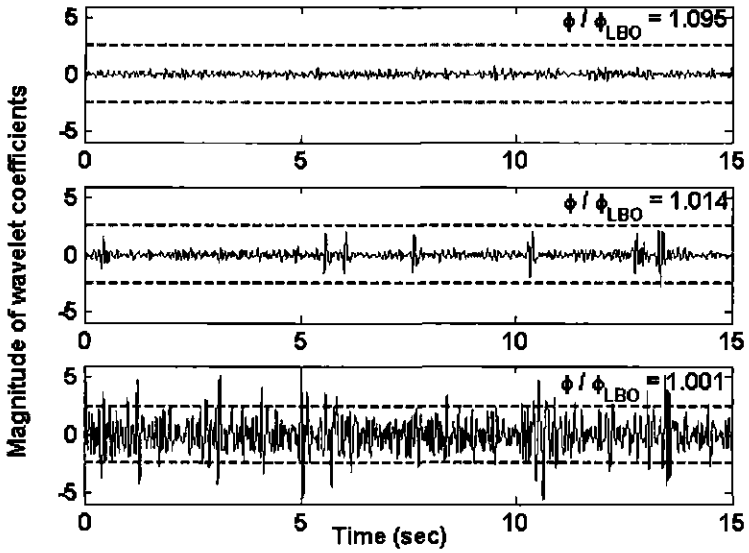

Figure 14. Time dependence of computed $W_3(t)$ wavelet coefficients of acoustic signal at a scale of 64 (~10 Hz) for $\phi/\phi_{LBO} = 1.095$, 1.014 and 1.001 from the swirl burner.

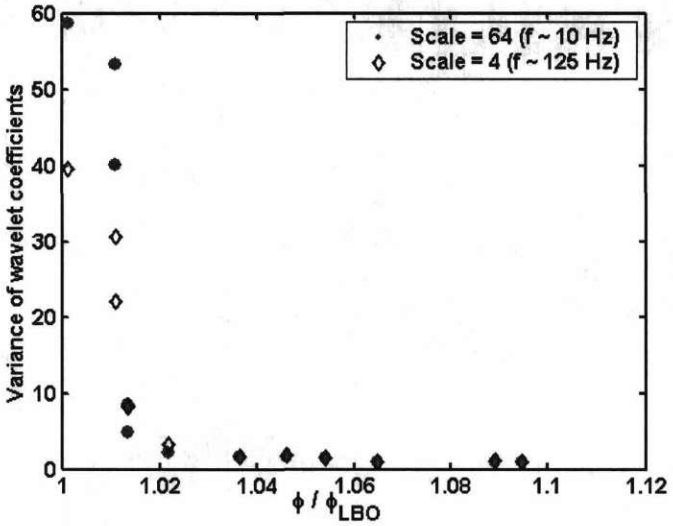

Figure 15. Dependence of $W_3(t)$ wavelet coefficient variance at scales of 64(~10 Hz) and 4 (~125 Hz) upon ϕ/ϕ_{LBO} for the swirl burner.

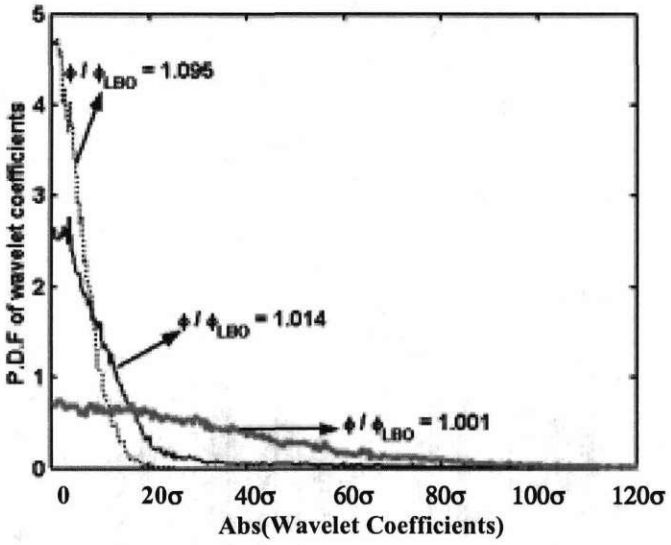

Figure 16. Wavelet transform PDF (using $W_3(t)$) from the swirl burner at a scale of 64(~10 Hz) for ϕ/ϕ_{LBO} = 1.095, 1.014 and 1.001.

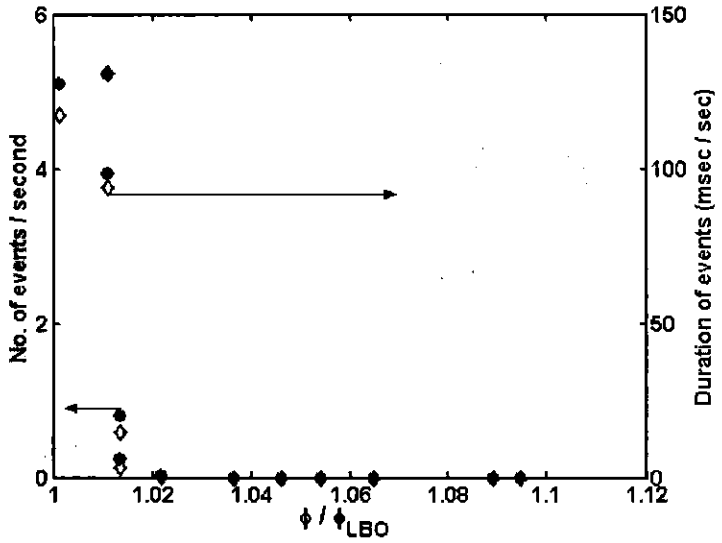

Figure 17. Dependence of the number and duration of events upon ϕ/ϕ_{LBO} in the swirl burner.

III.C LBO Control in a Liquid-Fueled Combustor

The primary goal for a LBO control actuator is to provide either an alternate stabilization mechanism for the flame or to increase the strength of the current stabilization point. Based on earlier success with actuation of the fuel distribution (e.g., piloting), a similar approach was adopted here. To accomplish this, we first looked at developing the optimal fuel distribution approach using passive (manual) control.

III.C.1 Pilot Fuel Development

From the high speed visualizations, it appears that the flame is anchored in the shear layer that lies between the two counter-rotating swirl flows. To enhance the "strength" of this stabilization region, the goal is to inject a larger fraction of the fuel (the "pilot" fuel) there. Since the current swirlers could not be easily modified to accommodate a pilot fuel injection in the separator lip, it was decided to inject the pilot fuel through one of the swirlers, upstream of the main fuel injector located in the center of the inner swirler. Again because of the inability to modify the production model swirlers, and restricted access to the burner head through the inlet section walls, we were limited to injecting the pilot fuel into the outer swirlers and to only one of the azimuthal flow passages. This azimuthal location resulted in the injected fuel leaving the swirler at thee top of the combustor. However, the swirler exit is located upstream of the point where the two swirling flows meet, thus the azimuthal location where the pilot fuel is actually injected into the combustor test section will likely be closer to the side of the combustor.

Two pilot fuel injectors were used: 1) a finely atomized, commercial macrolaminate injector and 2) a simple, pressure nozzle injector. The macrolaminate spray nozzle was located next to the inlet of the swirl vanes. The pressure nozzle was located at the entrance of the swirling passage. Figure 18 shows the effect of both the pilot configurations on the blowout limit of the combustor. The atomizer appears to have some decrease in blowout equivalence ratio at the lower pilot fractions, but loses its effect as the pilot fraction increases. The pressure nozzle on the

other hand, has a weaker effect at low pilot fractions, but continues to reduce the blowout equivalence ratio for higher pilot fractions. For both pilot injectors, visual observation of the flame suggests that there is near complete combustion of all the fuel entering the combustor. There is no significant change in the location of the visible flame radiation, and the flame does not extend beyond the combustor test section exit. Thus we conclude that piloting does in fact stabilize the overall combustion zone for equivalence ratios below the unpiloted blowout limit.

The differences behavior of the two injectors can be attributed to differences in their atomization characteristics. The macrolaminate injector produces good atomization of the fuel only for the higher pilot fractions (higher flow rates), which are closer to its designed operating range. At the high pilot fractions, the well atomized fuel spray may evaporate too quickly after coming in contact with the heated air or the hot metal of the swirlers. The pressure nozzle, on the other hand, produces a thin, poorly atomized, jet at all the flowrates (based on observations in quiescent conditions). Thus it should produce a less well mixed, less evaporated fuel flow.

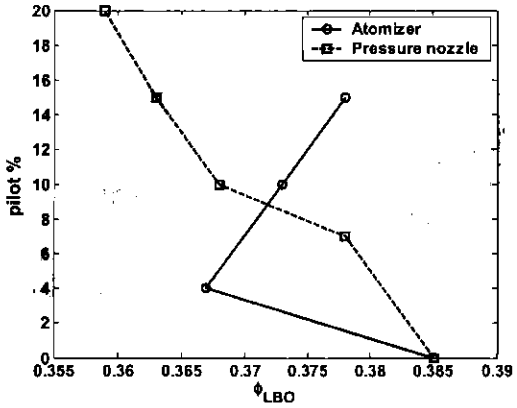

Figure 18. Variation of the blowout equivalence ratio with various pilot fractions for the two injector configurations investigated.

Redistribution of the fuel to the pilot requires that the main fuel flow be decreased (since the overall equivalence ratio is fixed). Thus the main combustion process is being deprived of fuel when the pilot fraction is increased. The pilot fuel is injected in order to increase the stabilization of the combustion process in some region of the combustor. If that region is stabilized *and* can in turn stabilize the rest of the combustor (which is less stable on its own due to the reduced main fuel flow), then the result is improved combustor stability and a decrease in the blowout equivalence ratio. Based on this reasoning, it appears that the fine atomization of the pilot fuel does not give an overall improved stabilization, while the poorly atomized pressure nozzle pilot does provide a useful tradeoff between pilot region stability and weaker combustion in the rest of the combustor.

In the current, non-premixed combustor, a decrease in (overall) blowout equivalence ratio of 6% was attained for a pilot fraction of ~15% (with the pressure nozzle). This can be compared to the earlier results for the premixed combustor, where the blowout equivalence ratio was reduced by 6% for only a 12% pilot fraction. Thus the effectiveness of the pilot is not as good in the current setup. This may be due to the fact that the pilot fuel is injected non-axisymmetrically in the current work. The azimuthal location of pilot injector was decided based on the ease of access and not based on the best possible injection point.

III.C.2 Effect of Pilot on LBO Sensing

Since the pilot injection can change the dynamics of the combustor near the LBO limit or change the spatial extent of the active combustion region, it might influence the efficacy of the LBO precursor sensing. Thus the effect of piloting on the sensing technique was investigated through open loop tests. Figure 19 shows the effect of pilot fraction on the LBO behavior, for the pressure nozzle only. As observed above the LBO limit (vertical lines) moves to leaner mixtures with increasing piloting. The average number of events detected per second as a function of equivalence ratio is also indicated for each pilot fraction case. The sensing approach described above successfully identifies precursor events with piloting. As in the unpiloted case, the number of events increases with a reduction of the overall equivalence ratio, i.e., as LBO proximity increases.

The earlier results from premixed gaseous combustor showed that higher pilot fraction increased the likelihood of events slightly at ϕ farther from the blowout limit and decreased it when the overall ϕ was closer to the blowout limit. Essentially, with increasing pilot fraction, the curve of events versus ϕ shifted to the left, with a small shift upwards at ϕ farther from LBO limit. Thus in the premixed combustor, the number of extinction events seen by a detector was a good indicator of increased combustor stability near blowout. In the non-premixed combustor, the results from fiber location 2, has a similar behavior as that from the premixed combustor. However, the results from fiber location 1 indicates that piloting decreases the blowout limit, while it appears to increase the occurrence of precursor events, for a given overall ϕ, compared to the no pilot case. In addition, the higher pilot fuel fraction (15%) produces less events than the low pilot case (7.3%).

To understand this discrepancy, one must remember that pilot fuel is not being injected axisymmetrically. Since fuel is only injected at one location around the circumference, it is likely that the improved stabilization is highly localized azimuthally in the combustor. If the detectors are not viewing this region (or not solely viewing this region), they are likely viewing areas with reduced ϕ, which are less likely to be stable. Since in the piloting method used, the injected pilot fuel tends to enter the combustor from the side rather than the top azimuthal location, fiber 2 has a higher chance of viewing the stabilized zone than fiber 1. Therefore, the observation of increased number of events with piloting could change if the pilot fuel were distributed more uniformly or if the sensing locations were changed.

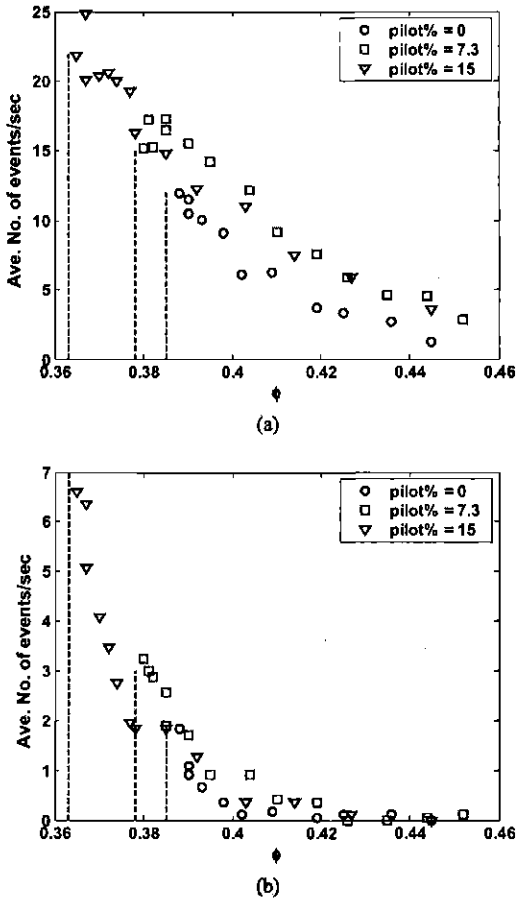

Figure 19. Variation of average number of events/sec with equivalence ratio for piloted and non piloted cases. (a) data from fiber 1, (b) data from fiber 2.

The previous work, in premixed combustor, used the control algorithm based on the number of precursor events per second. When the number of events increased as the LBO limit was approached, the pilot fraction was increased to make the combustor more stable. This decreased the number of precursors. Thus the control scheme had an objective to decrease the number of precursors by increasing the pilot fraction. In the non-premixed combustor, the same control approach can be used with the sensor location 2 since this signal behaves similar to that of the premixed combustor. On the other hand, with sensor location 1, the increased piloting does not decrease the number of events, but still makes the combustor stable. Yet since the pilot effectively moved the blowout limit away from the operating condition, this pilot can be used in a two state (ON/OFF) mode, to help the controller handle transient conditions where LBO limit is approached for a short duration.

III.C.3 Active Control Efforts

The LBO control experiments were performed in same setup described above, except in addition two computer controlled valves, driving electronics, and a control computer were installed to allow control of two independent, pressurized fuel systems dedicated to the main and pilot fuel lines, respectively (Figure 20). Each fuel line had a separate fuel tank, flow meter, and

computer-controlled flow valve. In the LBO control work performed in the previous NASA-supported effort, a single valve was used to govern the percentage of total fuel distributed among the pilot and main fuel lines. This approach was not feasible in the liquid fuel system since liquid fuel cannot be choked. Hence, the pressure drop from a split valve would alter the flow in the entire system.

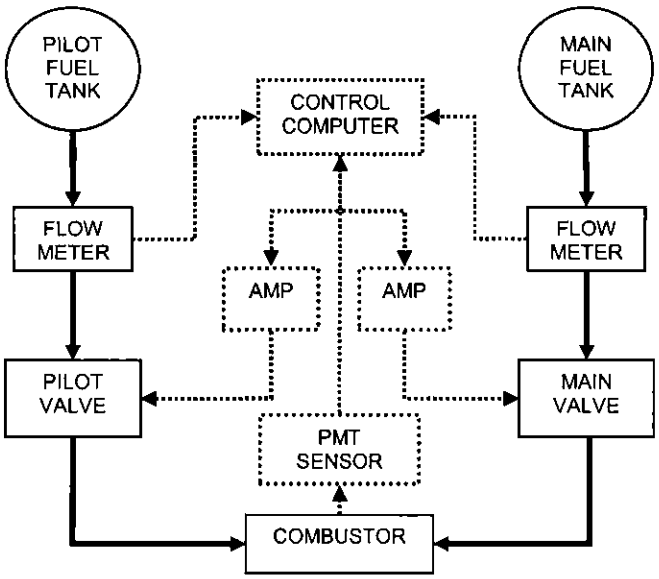

Figure 20. Signal and fuel flow schematic of controlled system.

The electronics to operate the valves were a source of some initial problems. The solenoid valves required 200 mA while the maximum current output from the control computer was 30 mA. Suitable amplifiers were procured for each of the valves but these had stability issues. The inductive load of the valve caused the amplified current to oscillate in a limit cycle. To rectify this, a capacitor was placed across the valve terminals, effectively eliminating the current oscillations. Next, the valves were calibrated in open loop, assuming that a given command voltage would always produce the same flow rate. The results of this calibration are given in Figure 21. Unfortunately, while the calibration appeared to follow a quadratic curve, the valve behavior shifted constantly. In order to prevent excessive (>10%) flow error, the valves had to be recalibrated every 5-10 minutes. Furthermore, the pilot valve could not operate for extended periods near the lower end of its flow range (about .06-.15 g/sec). It appeared that at low flow rates, the stream seemed to 'decay' without warning, i.e. the flow would suddenly drop sharply and stop altogether.

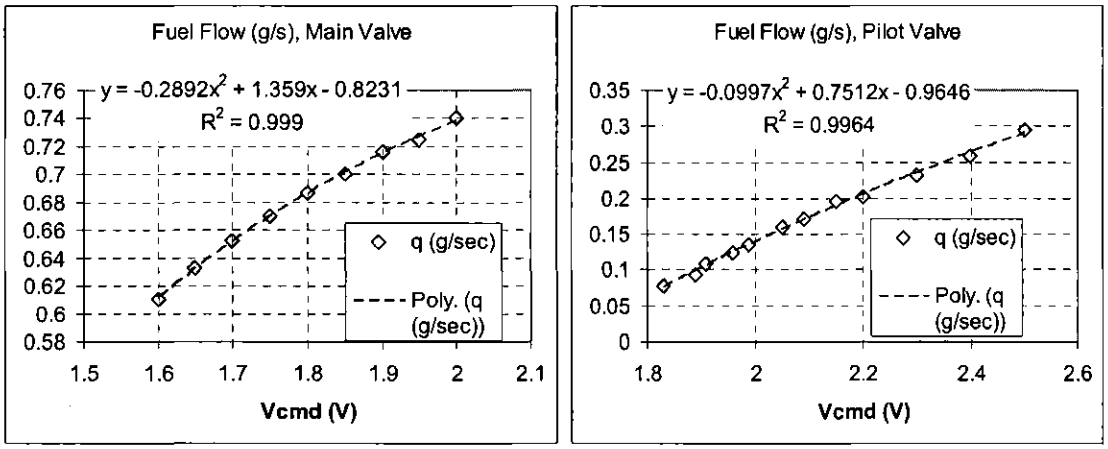

Figure 21. Initial calibration curves for the main and pilot valves.

In order to address the calibration and flow decay issues, an attempt was made to operate the valves in closed loop, using the flowmeter signal as feedback. However, the flowmeter signal was delayed by 2 seconds. Furthermore, increasing the voltage to the pilot valve when the flow started faltering did not prevent the flow decay. Upon closer inspection, it was determined that at low flow rates (the pilot was operated between 0.06 and 0.12 g/sec), the dissolved nitrogen in the pilot fuel precipitated into small bubbles (cavitation) that effectively reduced the injector opening. Although there were fewer bubbles when the pressure was reduced, the flow still decayed because the valve itself could not maintain the small aperture for more than 2 seconds. Even when the low flow rate was maintained, the turbine flowmeter often could not detect it. The minimum flow required for the flowmeter to detect a nonzero flow was anywhere between 0.04 to 0.06 g/s. Since the valve calibration was not valid for more than a few minutes even when there was no decay, and the flowmeter also was unable to detect the low flow rates, there was no way of knowing the pilot fuel flow rate within any reasonable degree of accuracy. Without knowledge of the flow rate, the constant overall fuel flow objective could not be met.

Since the problems with the pilot valve arose due to the extremely low flow rates, it was decided to split a higher pilot flow rate, with one split going into the injector and the other split directed into a bucket. This eliminated the flow meter and valve problems, however, calibration was a major issue. It was impossible to determine how much fuel was being injected and how much was being dumped at any given instance in time.

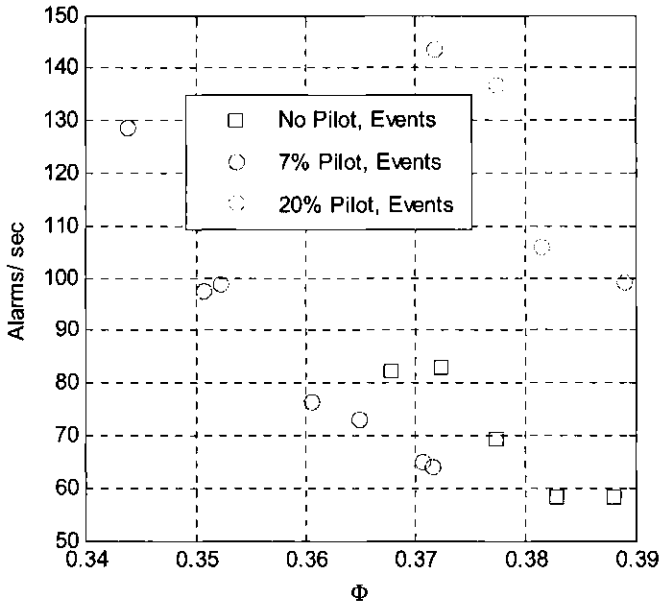

Figure 22. Open loop results. Alarms per second, on the y-axis, are the average number of detected precursors per second. Equivalence ratio is depicted on the x-axis.

Before the pilot flow ambiguity was known, an attempt was made to operate the combustor in open loop with different levels of fuel split. Figure 22 shows the data in a plot. The average number of precursors detected per second is shown on the y-axis while the equivalence ratio is the x-axis. If we neglect the pilot flow ambiguity problem, then we can say that 7% piloting improves margin while 20% piloting reduces it slightly. However, even though there is very little difference in the blowoff equivalence ratio between 0% and 20% piloting, the 20% case shows significantly more alarms.

Conceptually, if the combustor was operating with no pilot, and the alarms exceeded the allowable number, the controller would increase pilot fraction steadily. At 7% pilot, there would be a notable improvement, since the number of alarms would be lower at a particular equivalence ratio and the blowout limit would be shifted noticeably. However, if more actuation were required, and the controller responded by increasing pilot towards 20%, the situation would appear worse. There would now be more alarms at a given equivalence ratio. In response, the controller would increase piloting even further. Hence, there is an unstable, positive feedback loop. In an attempt to reduce alarms, piloting is increased and as a result, alarms increase as well.

The control actuation may be capped at 7% pilot in order to prevent this scenario and keep the combustor in the 'stable' regime. However, as noted previously, 7% pilot flow is nearly impossible to achieve with the control valve and nearly impossible to measure with the flow meter.

Therefore, closed-loop control was not achieved due to the many hardware related issues. Unreliable calibration, unsteady behavior of the solenoid valve at low flow rates, nitrogen bubble formation, and unresponsive flow meters all made determination of pilot flow rate impossible. If

the flow rates were higher, as with the main fuel line, the problems would not have been present. However, increasing the pilot beyond 7% placed the combustor control system in an unstable regime. Furthermore, the system did not allow the main flow to exceed 0.8 g/sec, so the maximum recommended pilot in that case would still only be 0.056 g/sec, and still within the problematic range.

IV. REFERENCES

[1]Correa, S.M., Power Generation and AeroPropulsion Gas Turbines: From Combustion Science to Combustion Technology, *Twenty Seventh Symposium (International) on Combustion*, The Combustion Institute, Pittsburgh, PA, 1998.

[2]McVey, J. B., Padget, F. C., Rosfjord, T.J., Hu, A.S., Peracchio, A.A., Schlein, B. and Tegel, D. R., "Evaluation of Low NOx Combustor Concepts for Aeroderivative Gas Turbine Engines," ASME paper 92-GT-133, presented at IGTACE, Cologne, Germany, June 1-4, 1992.

[3]Bowman, C.T., Control of Combustion-Generated Nitrogen Oxide Emissions: Technology Driven By Regulations, *Twenty Fourth Symposium (International) on Combustion*, The Combustion Institute, Pittsburgh, PA, 1992.

[4]Lefebvre, Arthur H., *Gas Turbine Combustion*, Ch. 9, Edwards Brothers: Ann Arbor, MI, 1999.

[5]DuBell, T.L., Cifone, A.J., "Combustor Influence on Fighter Engine Operability," AGARD Meeting on Mechanisms of Combustion Instability in Liquid Fueled Combustors.